ISSN 1062-8738, Bulletin of the Russian Academy of Sciences. Physics, 2016, Vol. 80, No. 1, pp. 68–73. © Allerton Press, Inc., 2016.
Original Russian Text © V.S. Berdnikov, K.A. Mitin, 2016, published in Izvestiya Rossiiskoi Akademii Nauk. Seriya Fizicheskaya, 2016, Vol. 80, No. 1, pp. 75–80.

Effect of Heat Transfer Mode on the Temperature and Thermal Stress Fields in Single Crystals

V. S. Berdnikov[a, b] and K. A. Mitin[a, b]

[a] *Kutateladze Institute of Thermal Physics, Siberian Branch, Russian Academy of Sciences, Novosibirsk, 630090 Russia*
[b] *Novosibirsk State Technical University, 630073 Russia*
e-mail: berdnikov@itp.nsc.ru

Abstract—Different modes of conjugate heat transfer in a crystal environment–growth chamber walls system with geometry similar to the upper part of a Czochralski thermal unit are investigated numerically. Calculations are performed for an argon Prandtl number of 0.68 and a Grashof number of 16000. The thermal stress fields in the crystal are calculated using the resulting temperature fields.

DOI: 10.3103/S1062873816010056

INTRODUCTION

The structural quality of single crystals grown using the pull-from-melt (Czochralski) technique depends on the shape and growth rate of the crystallization front. When growing a crystal, it is necessary to avoid sharp variations in its diameter and ensure the maximum symmetry of the temperature field and the minimum temperature gradients near the crystallization front [1]. A study of the convective heat exchange in a melt showed that melts with any Prandtl numbers are described by relations between dimensionless dynamic parameters, including the Grashof, Marangoni, and Reynolds numbers (*Gr*, *Re*, *Ma*), which characterize the intensity and relative role of free and forced convection at which the crystallization front will be a plane [2]. These conclusions have been confirmed in experiments with fusible substances. In [2], investigations were conducted ignoring heat transfer from the crystal to the environment. In the real high-temperature technological process, however, heat transfer has a complex conjugate character, and temperature fields are self-consistent over all of the growth chamber. Controlling the heat conditions of crystal growth is a fairly complicated problem, since the nonlinearity of convective and conjugate heat transfer between the crystal, melt, and environment requires that we solve the problem for numerous geometries of calculated areas during crystal growth.

In global simulations, such problems must be solved in a fully conjugated formulation, which requires near-impossible exact specification of the boundary conditions corresponding to the real process and a great deal of scarce computational and time resources. To understand general patterns of the dependence of temperature fields in crystals on the intensity of heat transfer from their generatrices and the corresponding thermal stresses, these problems can be solved by means of partial simulation. The results from such investigations are used to estimate the spatial dependence of the electric properties of a crystal on its growth conditions and heat prehistory. Heat transfer from the crystal to the growth chamber environment affects the temperature fields in the crystal and, in the conjugate heat transfer mode, alters the curvature of the front and determines the volume distribution of intrinsic point defects [1, 3] and other imperfections. Partial simulation, while not claiming to describe these processes fully, allows us to determine the main trends in the behavior of investigated systems upon varying certain control parameters or groups of parameters. Using the numerical method of finite differences [4], the authors investigated conjugate heat transfer in different modes. The relative role and interplay of heat conduction, convection, and radiation at different crystal lengths were studied.

FORMULATION OF THE PROBLEM

Considering the axial symmetry of the thermal units used for growing single crystals by the Czochralski technique, our calculations were performed in a two-dimensional (2D) region in cylindrical coordinates. The geometry of the calculated region corresponded to a simplified scheme of the upper part of the growth chamber consisting of a single crystal, seed crystal, rod, growth chamber walls, and screen separating the melt surface from the gas medium in the growth chamber. Buoyancy-driven convection was simulated using a dimensionless system of Navier–Stokes equations, energy, and discontinuity in the

Boussinesq approximation, described in vortex, current function, and temperature variables

$$\begin{cases} -\frac{1}{Pr}\left(\frac{\partial^2 T}{\partial r^2}+\frac{1}{r}\frac{\partial T}{\partial r}+\frac{\partial^2 T}{\partial z^2}\right)+u\frac{\partial T}{\partial r}+\upsilon\frac{\partial T}{\partial z}=0 \\ -\left(\frac{\partial^2 \omega}{\partial r^2}+\frac{1}{r}\frac{\partial \omega}{\partial r}+\frac{\partial^2 \omega}{\partial z^2}\right) \\ +u\frac{\partial \omega}{\partial r}+\upsilon\frac{\partial \omega}{\partial z}+\frac{\omega}{r^2}-u\frac{\omega}{r}=Gr\frac{\partial T}{\partial r} \\ -\left(\frac{\partial^2 \psi}{\partial r^2}+\frac{1}{r}\frac{\partial \psi}{\partial r}+\frac{\partial^2 \psi}{\partial z^2}\right)+\frac{\psi}{r^2}=-\omega \\ u=-\frac{\partial \psi}{\partial z}\quad \upsilon=\frac{1}{r}\frac{\partial (r\cdot\psi)}{\partial r} \end{cases}, \quad (1)$$

where T, ω, and ψ are the temperature, vortex, and current function, respectively, and u and υ are the radial and axial rate components, respectively.

In our dimensionless equations, $Gr = (\beta g/\nu^2)\Delta T R_S^3$ was the Grashof number. Here, β is the volume expansion coefficient of the gas, g is the gravitational acceleration, ν is the kinematic viscosity of argon, ΔT is the difference between the temperatures of the crystallization front and growth chamber walls, and R_S is the crystal's radius. The Prandtl number of argon is $Pr = \nu/a = 0.68$, where $a = \lambda_G/\rho C_P$ is thermal diffusivity, λ_G is thermal conductivity, ρ is density, and C_P is the specific heat at a constant pressure. The equations are reduced to dimensionless form using crystal radius R_S as the geometrical scale. The temperature difference ΔT was taken as our temperature scale. The rate scale was ν/R_S, and the radiation flux scale was $R_S^2/\lambda_G\Delta T$.

Radiation fluxes were calculated using the zone method [5] under the following assumptions: the calculated region is bounded by a closed system of surfaces; all of these surfaces are grey, diffusion-radiative and diffusion-reflective; the surfaces are divided into the area in which the radiation properties and temperature can be considered constant; and the medium filling the growth chamber is diathermic. In searching the thermal stress fields, a quasi-stationary problem of thermal elasticity was solved using the concept of a thermoelastic displacement potential [6]. The thermoelastic displacement potential can be obtained by solving the Poisson equation

$$\frac{\partial^2 F}{\partial r^2}+\frac{1}{r}\frac{\partial F}{\partial r}+\frac{\partial^2 F}{\partial z^2}=\frac{1+\mu}{1-\mu}\alpha T, \quad (2)$$

where F is the thermoelastic displacement potential, μ is the Poisson coefficient, and α is the thermal expansion coefficient. The thermal stress field can be found from the distribution of the thermoelastic displacement potential using the relation

$$\sigma_{ij}=\frac{E}{1+\mu}\left(\frac{\partial^2 F}{\partial i\partial j}-\Delta F\delta_{ij}\right), \quad \delta_{ij}=\begin{cases}1 \text{ at } i=j,\\ 0 \text{ at } i\neq j,\end{cases} \quad (i,j=r,z,\varphi). \quad (3)$$

Here, σ is thermal stress, E is Young's modulus, Δ is a Laplacian, and δ_{ij} is the Kronecker symbol. The Von Mises equivalent stress is determined as [6]

$$\sigma_i=\sqrt{\frac{(\sigma_{rr}-\sigma_{zz})^2+(\sigma_{rr}-\sigma_{\varphi\varphi})^2+(\sigma_{zz}-\sigma_{\varphi\varphi})^2+6(\sigma_{rz}^2+\sigma_{r\varphi}^2+\sigma_{z\varphi}^2)}{2}}. \quad (4)$$

The problem was solved at the following boundary conditions: The maximum temperature in the system (1683 K) was specified at the crystallization front: $T|_{\Gamma_1}=1$. The thermal isolation, impermeability, and adhesion conditions $\left.\frac{\partial T}{\partial n}\right|_{\Gamma_2}=0$, $\psi|_{\Gamma_2}=0$, $\omega|_{\Gamma_2}=\left.\frac{\partial V_r}{\partial z}\right|_{\Gamma_2}$, were specified on the screen separating the melt surface from the growth chamber. On the growth chamber walls, the minimum temperature in the system was maintained and the impermeability and adhesion conditions were specified: $T|_{\Gamma_3}=0$, $\psi|_{\Gamma_3}=0$, and $\omega|_{\Gamma_3}=-\left.\frac{\partial V_z}{\partial r}\right|_{\Gamma_3}$. On the crystal's generatrices, the impermeability, adhesion, and ideal contact conditions were specified with regard to the radiation fluxes: $\psi|_{\Gamma_4}=0$, $\omega|_{\Gamma_4}=\left.\frac{\partial V_r}{\partial z}\right|_{\Gamma_4}-\left.\frac{\partial V_z}{\partial r}\right|_{\Gamma_4}$, $T|_{\Gamma_{4-}}=T|_{\Gamma_{4+}}$, $-\lambda_S\left.\frac{\partial T}{\partial n}\right|_{\Gamma_{4-}}=-\lambda_G\left.\frac{\partial T}{\partial n}\right|_{\Gamma_{4+}}+Q$. The normal stress on all crystal surfaces was zero: $\sigma_{nn}|_\Gamma=0$.

The numerical simulation was performed using the method of finite differences on a nonuniform mesh of 101×501 nods, consisting of triangular finite elements with specified linear functions. The calculations were performed for two values of the crystal's thermal conductivity: at low thermal conductivity $\lambda_S^L = 1.51\ \mathrm{W\,m^{-1}\,K^{-1}}$ typical of oxide single crystals and at high thermal conductivity $\lambda_S^H = 26\ \mathrm{W\,m^{-1}\,K^{-1}}$ typical of single-crystal silicon. The crystal's radius was $R_S = 0.05$ m, the thermal conductivity of argon was $\lambda_G = 5.83\times 10^{-2}\ \mathrm{W\,m^{-1}\,K^{-1}}$, the thermal expansion coefficient of the gas was $\beta = 6.4\times 10^{-4}\ \mathrm{K^{-1}}$, and the kinematic viscosity of the gas was $\nu = 2.54\times 10^{-4}\ \mathrm{m^2\,s^{-1}}$. The properties of argon were those observed at a temperature of 1600 K [7]. The emissivity of all the surfaces in the system was 0.5. The

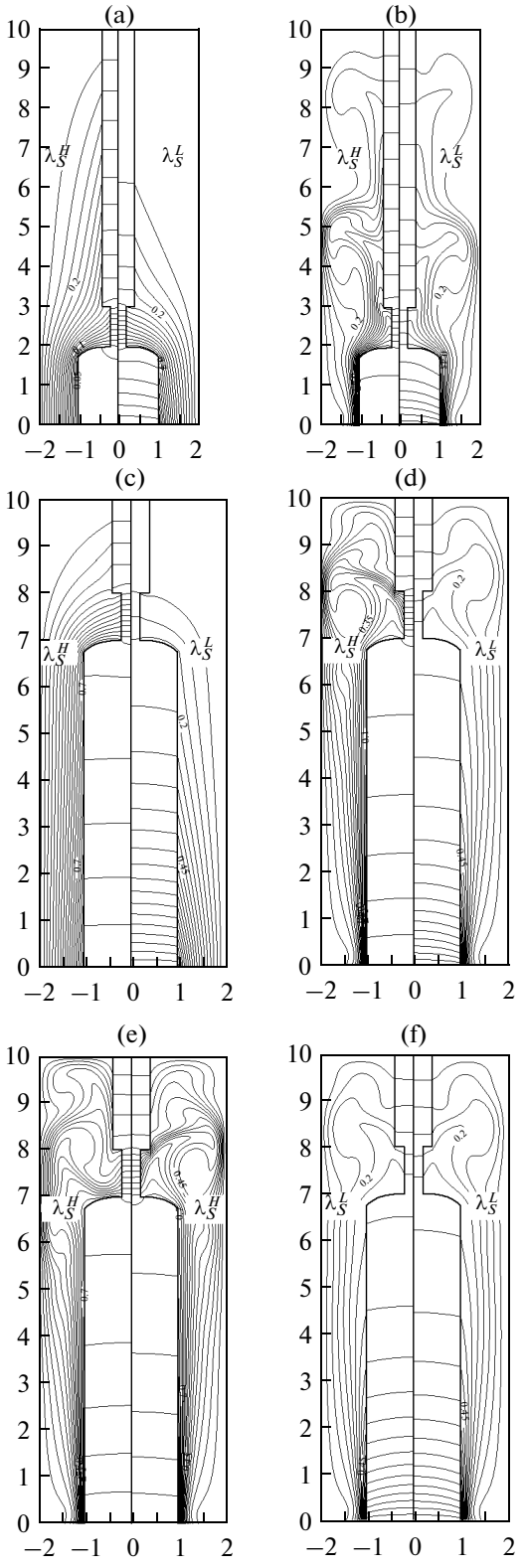

Fig. 1. Isoterms in different heat transfer modes at low (λ_S^L) and high (λ_S^H) thermal conductivities and different lengths of the crystal in (a, c) the conductive, (b, d) radiation–convective, (e, f) convective (on the left), and radiation–convective (on the right) modes.

Poisson coefficient was $\mu = 0.25$, the linear expansion coefficient of the crystal was $\alpha = 5.2 \times 10^{-6}$ K^{-1}, and Young's modulus was $E = 1.59 \times 10^{11}$ Pa.

RESULTS AND DISCUSSION

We performed calculations in the conductive, radiation-conductive, convective, and radiation-convective modes of heat transfer from the crystal at Grashof number $Gr = 16000$, which corresponds to temperature difference $\Delta T = 1330$ K in the relative crystal length range of $1 \le H_S/R_S \le 8$. The temperature fields in the crystal depended largely on the heat transfer mode. The temperature field in a compound body was determined by solving the heat-conduction equation for all heat transfer modes. When analyzing the relative role of different heat transfer mechanisms, it is logical to consider heat conduction over the entire calculated area to be the initial mode. In preliminary engineering calculations, only the heat-conduction equations over the entire composite area are often solved. In this mode, the calculated temperature field in a solid is naturally taken as a base for comparison and understanding the effect of convective and radiation heat transfer from the crystal's generatrices and the entire crystal–seed–rod compound body.

According to the data calculated in the conductive mode at high thermal conductivity, the temperature field in the crystal is strongly nonuniform (Fig. 1). Consequently, the distribution of radial and axial temperature gradients in different crystal parts is also nonuniform. This results in nonuniform radial distributions of the axial local heat fluxes, which is especially pronounced at the lower heated end (model crystallization front) and in the upper part of the crystal, where the region of transition from the crystal to the seed plays an important role. At the low thermal conductivity of the crystal, the axial and radial temperature gradients increase sharply at the crystal's base. This can be seen clearly in the shape of isotherms and their crowding near the crystallization front.

In the convective heat transfer mode, the area near the crystal's base is cooled more effectively. As a result, the axial temperature gradients in the lower part of the crystal grow considerably, due to the descending cold gas flows formed on the cold growth chamber walls turning in the lower part of the gas layer and flowing onto the hot crystal base. The gas is then heated and flows upward along the crystal generatrix under the action of buoyancy. Afterwards, the gas flows are cooled on the growth chamber walls and fall back onto the crystal's base. Convective heat transfer thus leads to a sharp increase in the axial gradients in the hot parts at the crystal's base. However, depending on the calculated area geometry, it can lead to a reduction in the temperature gradients in colder crystal parts due to heating by the ascending hot gas flux. Interestingly, the intensity of the cold gas flux flowing onto the crystal base depends less on the thermal conductivity of the crystal (Fig. 2).

At low thermal conductivity, the spatial shape of convective flows is retained, but their intensity in the region above the crystal decreases. This is because a crystal with higher thermal conductivity removes heat from the crystallization front much better, and the upper part of the crystal is consequently heated to higher temperatures. In addition, the amplitude of the axial component of the rate in the gap between the crystal and growth chamber enclosure falls. As the thermal conductivity of the crystal is reduced, the temperature difference between the crystallization front and upper end of the crystal increases. As a result, the ascending gas flows can effectively heat the upper part of the crystal when its length is increased.

Allowing for the radiation flows appreciably changes the temperature distribution over the surface and inside the crystal in both the conductive and convective heat transfer modes, and the local heat flows on the crystal's surface are greatly intensified. The efficiency of cooling increases over the entire crystal volume, as is indicated by the crowding of isotherms at the crystal's base. The temperature on the crystal's genetratrices falls. Hence, the difference between the temperatures of the cold growth chamber walls and the crystal surface's is reduced. As a result, the intensity of convection currents falls somewhat at a specified characteristic ΔT (Gr) value.

As the crystal's length is increased, the axial temperature gradients at its base change in all modes (Fig. 3). At high thermal conductivity of the crystal, the axial gradients grow almost linearly along with the crystal's length (Figs. 3a and 3c), while at low thermal conductivity, the growth of the axial temperature gradient slows as the crystal's height increases (Fig. 3d). Starting from a certain length, the axial gradients change negligibly upon a further increase in the crystal's height. In addition, it should be noted that the axial temperature gradients increase notably with a drop in thermal conductivity (Fig. 3d).

In all modes, the axial temperature gradients exhibit a nonuniform radial distribution. Their maximum near the crystallization front lies on the crystal's generatrices. This is especially pronounced in the convective heat transfer mode, when the radial temperature gradients increase because of the cold gases flowing onto the base in the lower part of the crystal. With convective heat transfer and low thermal conductivity, the growth of the axial gradient first slows and then stops as H_S/R_S rises. In addition, the axial temperature gradient maximum shifts from the surface to the center of the crystal as the distance to the crystallization front grows. This is especially pronounced in crystals with low thermal conductivity, since a substantial fraction of the heat is transferred via thermal conductivity from a single crystal to a seed crystal with a much smaller diameter.

Thermal stresses are also nonuniformly distributed over the crystal volume. It is interesting that as the length of the crystal grows, the Von Mises equivalent stresses at the crystal's base first increase and then start to fall (Fig. 4). This is observed most clearly in crystals

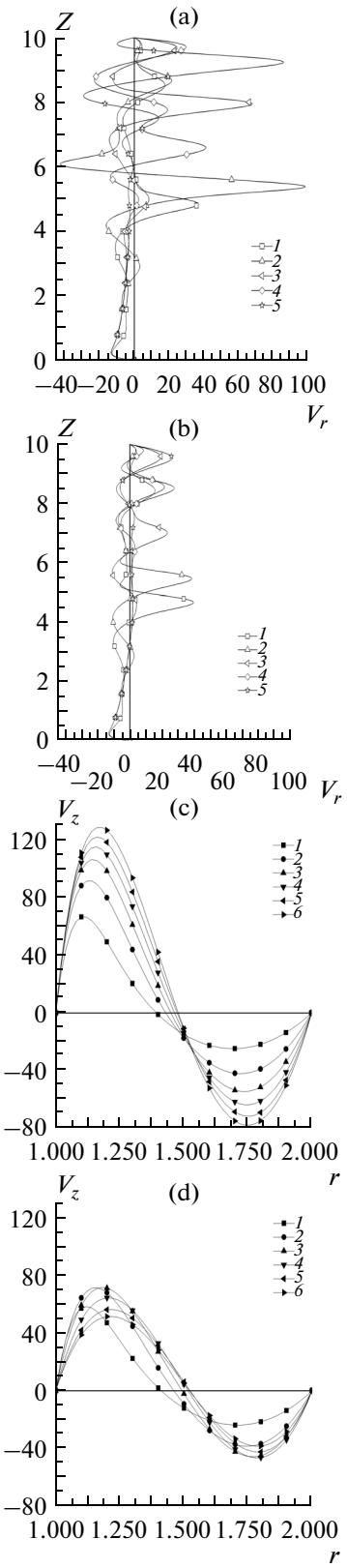

Fig. 2. Radial rate component profiles in cross section $r = 1.5$ at (a) high and (b) low thermal conductivity of the crystal and lengths (*1*) $H_S/R_S = 1$, (*2*) 3, (*4*) 7, and (*5*) 8. Axial rate profiles at (c) high and (d) low thermal conductivity of the crystal and length $H_S/R_S = 8$ in cross sections (*1*) $z = 1$, (*2*) 2, (*3*) 3, (*4*) 4, (*5*) 5, and (*6*) 6.

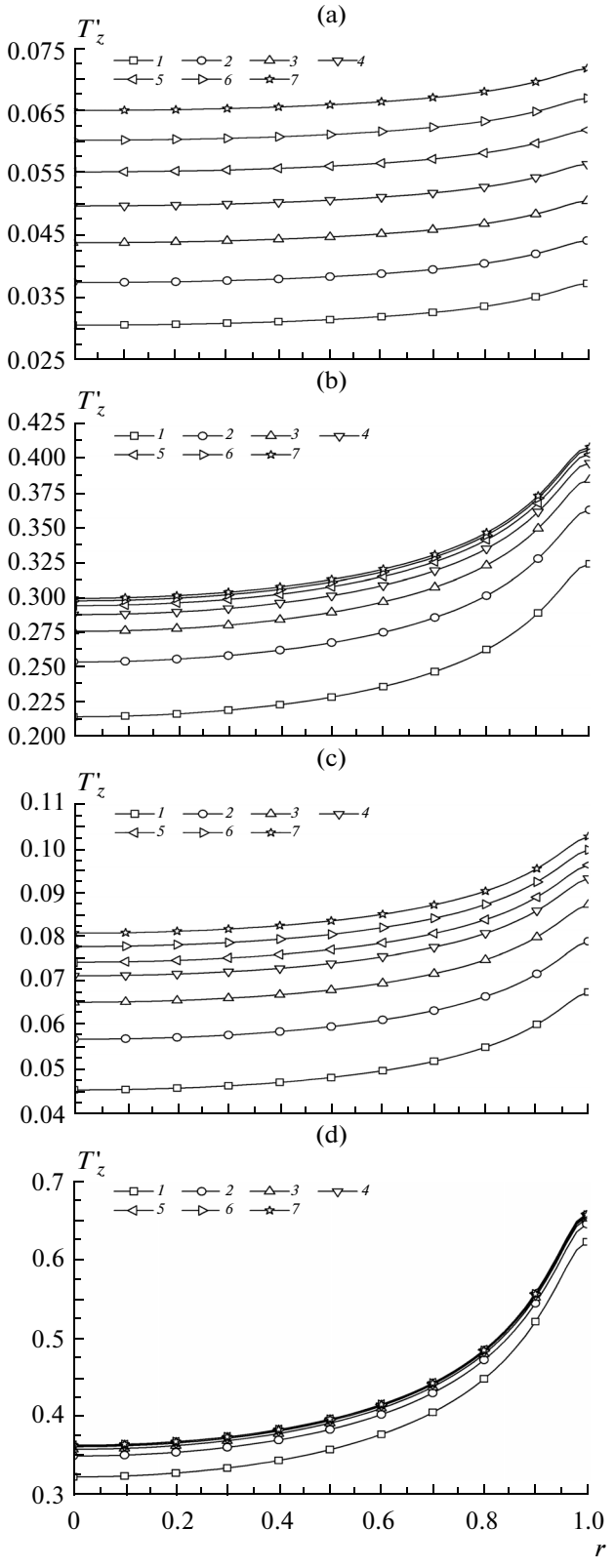

Fig. 3. Axial temperature gradient profiles in cross section $z = 0.04$ in the (a, b) radiation–conductive and (c, d) radiation–convective heat transfer modes at (a, c) high and (b, d) low thermal conductivity of the crystal and lengths (*1*) $H_S/R_S = 2$, (*2*) 3, (*3*) 4, (*5*) 6, (*6*) 7, and (*7*) 8.

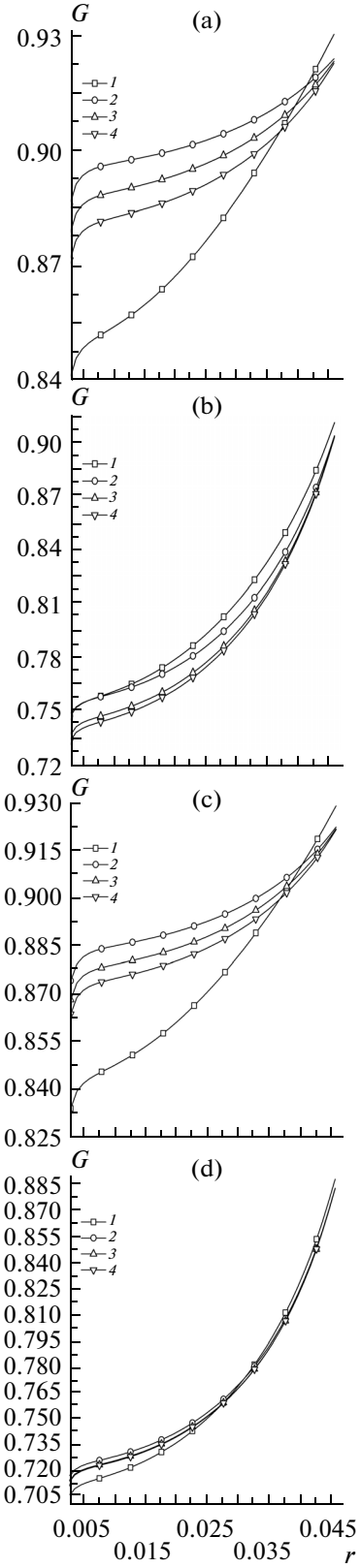

Fig. 4. Von Mises equivalent stress distribution profiles in cross section $z = 0.04$ in (a, b) the radiation–conductive and (c, d) radiation–convective heat transfer modes at (a, b) high and (b, d) low thermal conductivity of the crystal and lengths (*1*) $H_S/R_S = 2$, (*2*) 4, (*3*) 6, and (*5*) 7.

with high thermal conductivity. In addition, thermal stresses fall somewhat upon a reduction in thermal conductivity.

The maximum on the curves of the radial distribution of thermal stresses at the crystallization front lies on the crystal generatrix and coincides with the maxima of the axial and radial temperature gradients. It can be seen that in the convective heat transfer mode, the thermal stresses at the crystallization front are reduced.

CONCLUSIONS

The temperature fields in crystals depend largely on the mode of heat transfer. Calculations of the temperature fields in crystals in the heat conduction mode provide an excessively rough approximation. Convective heat transfer greatly affects the temperature distribution in crystals and leads to efficient cooling of a crystal's base. This is because gas flows cooled on cold growth chamber walls flow onto the hot crystal's base. As a result, the axial and radial temperature gradients at the crystal's base grow appreciably. Radiation heat transfer greatly changes the temperature distribution on the surface and inside the crystal in both the conductive and convective heat transfer modes. Local heat flows from the crystal's lateral surface increase dramatically. The contribution from convective heat transfer is also important upon radiation–convection heat transfer from the crystal's surface. The radial distributions of thermal stresses do not qualitatively change upon variations in the thermal conductivity of the crystal, but at high thermal conductivity, thermal stresses at the crystal's base fall monotonically as the length of the crystal grows, while at lower thermal conductivity, they depend more weakly on the crystal's length and the dependence is reversed; i.e., it first rises and then falls.

ACKNOWLEDGMENTS

This work was supported by the Siberian Branch of the Russian Academy of Sciences, project no. III.18.2.5, state reg. 01201350443; and by the Russian Foundation for Basic Research, project no. 15-08-07991.

REFERENCES

1. Mil'vidskii, M.G., *Poluprovodnikovye materialy v sovremennoi elektronike* (Semiconductor Materials in Modern Electronics), Moscow: Nauka, 1986.
2. Berdnikov, V.S., Vinokurov, V.A., Vinokurov, V.V., and Gaponov, V.A., *Tepl. Protsessy Tekh.*, 2011, vol. 3, no. 4, p. 177.
3. Prostomolotov, A.I. and Mil'vidskii, M.G., *Izv. Vyssh. Uchebn. Zaved. Mater. Elektron. Tekh.*, 2008, no. 3, p. 49.
4. Soloveichik, Yu.G., Royak, M.E., and Persova, M.G., *Metod konechnykh elementov dlya resheniya skalyarnykh i vektornykh zadach* (Finite Element Method for Solving Scalar and Vector Problems), Novosibirsk: Novosib. Gos. Tekh. Univ., 2007.
5. Sparrow, E.M. and Cess, R.D., *Radiation Heat Transfer*, CRC Press, 1978.
6. Melan, E. and Parcus, H., *Thermal Expansions in Stationary Temperature Fields*, Wien, 1953.
7. Vargaftik, N.B., *Spravochnik po teplofizicheskim svoistvam gazov i zhidkostei* (Handbook on Thermal Physical Properties of Gases and Fluids), Moscow: Nauka, 1972.

Translated by E. Bondareva